Communication

Ribosyl Geometry in the Transition State of *Streptococcus pneumoniae* Methylthioadenosine Nucleosidase from the 3#-H Kinetic Isotope Effect

Minkui Luo, and Vern L. Schramm

J. Am. Chem. Soc., **2008**, 130 (35), 11617-11619 • DOI: 10.1021/ja804578m • Publication Date (Web): 12 August 2008

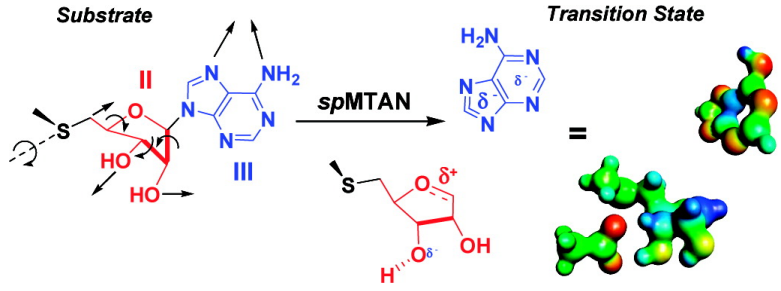

More About This Article

Additional resources and features associated with this article are available within the HTML version:

- Supporting Information
- Access to high resolution figures
- Links to articles and content related to this article
- Copyright permission to reproduce figures and/or text from this article

View the Full Text HTML

J|A|C|S COMMUNICATIONS

Published on Web 08/12/2008

Ribosyl Geometry in the Transition State of *Streptococcus pneumoniae* Methylthioadenosine Nucleosidase from the 3′-^{2}H Kinetic Isotope Effect

Minkui Luo and Vern L. Schramm*

Department of Biochemistry, Albert Einstein College of Medicine, 1300 Morris Park Avenue, Bronx, New York 10461

Received June 16, 2008; E-mail: vern@aecom.yu.edu

Transition state (TS) structures of enzymatic reactions provide information for developing tight-binding inhibitors.[1,2] Stable analogues, if perfectly mimicking an enzymatic transition state, can bind the enzyme $10^{10}-10^{16}$ tighter than its substrate.[3,4] These affinities achieve the ultimate goal of noncovalent irreversible binding for enzyme inhibition. A surprise in the field of enzymatic transition state analysis is that closely related enzymes can form distinct transition states.[5−10] For example, mutations of purine nucleoside phosphorylases remote from the catalytic sites cause differences in their TS structures.[8] Kinetic isotope effects (KIEs) together with computational chemistry have provided a powerful approach to elucidate enzymatic TS structures.[2,11] Current efforts in this field are to use remote isotope effects to explore the geometric and electrostatic features of enzymatic transition states in greater detail.[9,12−14,15a]

Methylthioadenosine nucleosidases (MTANs) function in bacterial purine/methionine salvage and quorum sensing via irreversible degradation of 5′-methylthioadenosine (MTA) into adenine and 5-methylthioribose (Figure 1).[14,16,17] These important biological functions have led us to develop TS analogue inhibitors as potential antibiotics against various MTANs.[18,19] Our interest in MTAN transition states was also stimulated by the finding that MTAN isozymes form structurally distinct transition states.[14,16] So far, the MTAN transition state structures have been solved without constraint of the 3′ geometry.[13,14,15a] Knowledge of the 3′ KIE would enhance MTAN TS structural detail, since the 3′ KIE reports on 3′-hydroxyl polarization and ribosyl pucker at MTAN transition states.[15a] Finally, it has been proposed, but not directly tested by KIE approaches, that MTAN catalytic mechanisms involve 3′-OH ionization.[15] Here we extend TS analysis for *Streptococcus pneumoniae* MTAN (*sp*MTAN) by direct measurement of its [3′-^{2}H] KIE. The [3′-^{2}H] KIE is consistent with a unique H3′-*endo*→*exo* configuration and 3′-hydroxyl polarization without full ionization at the *sp*MTAN TS. New structural detail at the *sp*MTAN TS is revealed by including the [3′-^{2}H]MTA KIE in the family of intrinsic isotope effects.

Intrinsic [1′-^{3}H], [2′-^{3}H], [4′-^{3}H], [5′-^{3}H$_2$], [1′-^{14}C], and [9-^{15}N] KIEs of *sp*MTAN-catalyzed hydrolysis were reported previously (Table 1).[15a] Here we synthesized [3′-^{2}H]MTA derivatives (Supporting Information) and measured the key [3′-^{2}H] KIE to extend the TS determination (Table 1 and Supporting Information). KIE experiments were carried out under competitive conditions with [8-^{14}C] as the remote label of the heavy isotopic substrate ([3′-^{2}H, 8-^{14}C]MTA) and [2,8-^{3}H$_2$]MTA as its [3′-^{1}H] competitive isotopic pair. The V_{max}/K_m [3′-^{2}H] KIE was obtained by correcting the experimental [2,8-^{3}H$_2$] KIE, which was determined with [2,8-^{3}H$_2$]/[8-^{14}C]MTAs as the competitive substrates. The V_{max}/K_m [3′-^{2}H] KIE was corrected for forward commitment $C_f = 0.121$[15a] to give a [3′-^{2}H] intrinsic KIE of 1.020 ± 0.006.

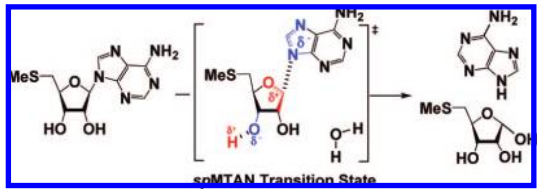

Figure 1. *sp*MTAN-catalyzed hydrolysis. *sp*MTAN hydrolyzes MTA into adenine and 5-methylthioribose through the proposed TS. Substrate synthesis is described in Figure S1 and Supporting Information.

Table 1. Intrinsic and Computational KIEs of *sp*MTAN TS and Its Candidate

	intrinsic KIEs vs computational KIEs		
		computational KIEs[b]	
isotope labeling	intrinsic KIEs[a]	unpolarized TS candidate[c]	spMTAN TS[d]
[9-^{15}N]	1.037 ± 0.004	1.035[e]	1.035[e]
[1′-^{14}C]	1.000 ± 0.005	1.001	1.001
[1′-^{3}H]	1.235 ± 0.002	1.363	1.374
[2′-^{3}H]	1.095 ± 0.002	1.074	1.096
[3′-^{2}H]	1.020 ± 0.006	0.943	1.020
[4′-^{3}H]	1.003 ± 0.005[f]	0.960	1.000
[5′-^{3}H$_2$][g]	1.019 ± 0.002	0.987 [proR,S]	1.010 [proR,S]
		1.012 [proR]	1.015 [proR]
		0.976 [proS]	0.996 [proS]

[a] KIEs corrected for commitment factors. [3′-^{2}H] KIE and [4′-^{3}H] KIE were determined in this work, and the rest were reported.[15] [b] Computational KIEs of MTAN TS candidates. [c] The *sp*MTAN TS without acetate anion (3′-OH polarization effect). [d] Intrinsic KIEs were used as constrains. [e] Theoretical maximum for the [9-^{15}N] KIE.[15a, S4] [f] The [4′-^{3}H] KIE was measured 6 times. The present KIE matches the previous [4′-^{3}H] KIE[15] within error and fit the computational KIE. [g] KIEs of *pro-R* and *pro-S* ^{3}H were calculated, and their products were reported as the [5′-^{3}H$_2$] KIE.

We then refined the *sp*MTAN TS structure by incorporating the [3′-^{2}H] intrinsic KIE with the [1′-^{3}H], [2′-^{3}H], [4′-^{3}H], [5′-^{3}H$_2$], [1′-^{14}C], and [9-^{15}N] KIEs (Table 1) as constraints to match *sp*MTAN TS candidates (Supporting Information). An acetate anion was included adjacent to the MTA 3′-OH moiety during modeling to mimic the interaction between the 3′-OH and *sp*MTAN E174.[19] Systematically altering C1′−N9, O3′−O^{carboxyl} distances and dihedral angles influencing [1′-^{3}H], [2′-^{3}H], [3′-^{2}H], [4′-^{3}H], and [5′-^{3}H$_2$] KIEs identified the best match to the KIEs and is assumed to represent the *sp*MTAN TS (Figure 2).

The *sp*MTAN TS is a fully dissociative (S_N1), ribooxacarbenium-like structure with its C1′−N9 distance larger than 3.2 Å (Figure 2). The ribosyl moiety adopts a H3′-*endo*→*exo* transition conformation, and the 3′-OH residue is partially polarized by the adjacent carboxylate with a hydrogen bond distance of 2.83 Å (Figures 2,3). The dissociative S_N1 character of the *sp*MTAN TS is consistent with the [1′-^{14}C] KIE of unity and the large [1′-^{3}H] KIE of 1.24

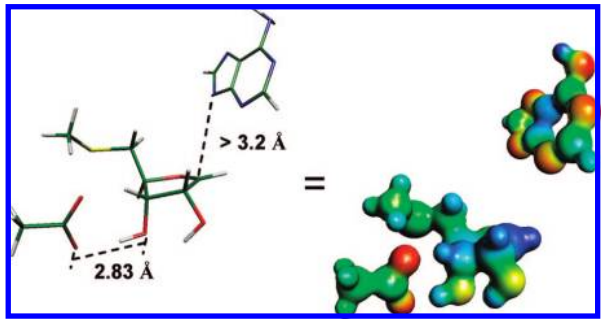

Figure 2. *sp*MTAN transition state structure with acetate near O3′ (stick and MEP models). The TS is a fully dissociated adenylate anion (C1′−N9 distance > 3.2 Å), partially polarized 3′-OH (O3′−$O^{carboxyl}$ = 2.83 Å), and a H3′-*endo*→*exo* ribosyl pucker. The CUBE subprogram of Gaussian 98 was used to generate molecular electrostatic potential (MEP) surfaces, which are visualized using Molekel 4.0.

(Table 1), a pattern that has been well established among N-ribosyl transferase enzymes.[14−16,20] The full C1′−N9 bond dissociation (>3.2 Å) at the *sp*MTAN TS is also supported by its close-to-theoretical maximum [9-^{15}N] KIE (Table 1).[15a]

The extent of 3′-OH polarization at the *sp*MTAN TS is determined by the magnitude of the [3′-^{2}H] KIE. The significant [3′-^{2}H] KIE of 1.020 constrains the O3′−$O^{carboxyl}$ hydrogen bond to a distance of 2.83 Å (Figure 2). The O3′−$O^{carboxyl}$ interaction polarizes the 3′-hydroxyl by increasing the OH bond length (0.97 Å in MTA vs 1.02 Å at the TS). Polarization of the 3′-OH at the *sp*MTAN TS is required to account for the [3′-^{2}H] KIE of 2%. Removing this interaction reduces the KIE to an inverse 6% (Table 1). Full ionization of the 3′-OH as proposed for *E. coli* MTAN would generate a [3′-^{2}H] KIE larger than 12% and can be excluded for the TS of *sp*MTAN.

The ribosyl pucker at the *sp*MTAN TS is nearly planar with the corresponding C4′ and C2′ dihedral angles between those of the unrestrained H3′-*endo* substrate and a fully developed H3′-*exo* ribooxacarbenium ion (Figure 2,3). This *endo*→*exo* intermediate configuration was derived from the combined [4′-^{3}H], [2′-^{3}H], [3′-^{2}H], and [5′-$^{3}H_2$] KIEs as discussed below.

The [4′-^{3}H] KIE constrains possible C3′−C4′ geometries at the *sp*MTAN TS (O3′−C3′−C4′−H4′ dihedral angle). The [4′-^{3}H] KIE is related to 3′-OH polarization and the C4′ TS configuration. With the known 3′-OH polarization, the 4′-CH-adjacent dihedral angles were varied systematically to match the intrinsic [4′-^{3}H] KIE 1.003 (Supporting Information). The resulting C4′ configuration features a small, repulsive O3′−C3′−C4′−H4′ dihedral angle of 10° (−36° for unrestricted MTA, Figures 2, 3). For MTAN transition states without the corresponding C4′-gauche interaction and 3′-OH polarization, [4′-^{3}H] KIEs are inverse 6%. We calculated that the unfavorable O3′−C3′−C4′−H4′ dihedral angle causes a 2− 3% [4′-^{3}H] KIE and the adjacent 3′-OH polarization contributes another 4% [4′-^{3}H] KIE (Table 1).

The [2′-^{3}H] KIE reflects C2′−H2′ hyperconjugation with the C1′−2p_z orbital at the *sp*MTAN TS (H1′−C1′−C2′−H2′ dihedral angle).[13,14] The degree of hyperconjugation was examined by altering H1′−C1′−C2′−H2′ dihedral angles stepwise to match the intrinsic [2′-^{3}H] KIE of 1.095. The corresponding H1′−C1′−C2′−H2′ dihedral angle is 59°, indicating a modest C2′−H2′ hyperconjugation at the *sp*MTAN TS.[13,15,20] The 9.5% [2′-^{3}H] KIE includes 7.5% from the C−H hyperconjugation and 2% from the partial 3′-OH polarization. The two effects were resolved by the 2% decrease in the [2′-^{3}H] KIE upon removing the 3′-OH polarization (Table 1).

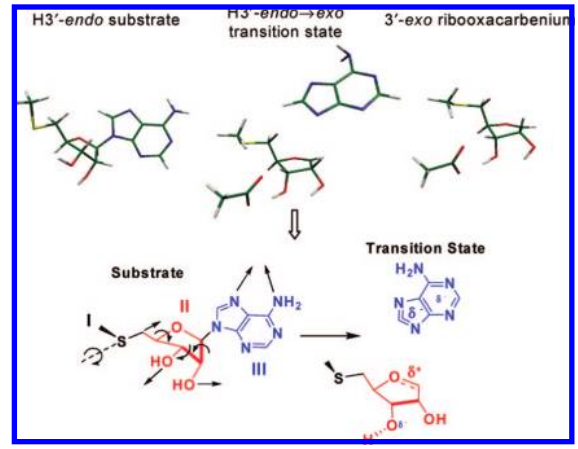

Figure 3. Dynamic motions of *sp*MTAN-catalyzed hydrolysis. The upper panel compares the structures of free H3′-*endo* MTA (substrate), H3′-*endo*→*exo* TS, and H3′-*exo* oxacarbenium intermediate. The lower panel indicates atomic motions as MTA evolves into the TS. The conformation of region **I** (black) is fixed following formation of the Michaelis complex. Purine dissociation (region **III**, blue) is rapid, followed by the relatively slow reconfiguration of region **II** (red). The arrows display the proposed motions.

The 5′-geometries at the *sp*MTAN TS were modeled from the [5′-$^{3}H_2$] KIE of 1.019. The TS structure has the 5′-methylthio moiety close to the 3′-OH group. The O4′−C4′−C5′−S dihedral angle at the *sp*MTAN TS is 156°, placing the 5′-methylthio opposite the ribosyl 4′-ring oxygen. The 5′ geometries extracted from other MTAN transition states or MTAN-bound transition-state analogues[13−15,19,21] gave variable [5′-$^{3}H_2$] KIEs and were not further analyzed.

Here we incorporated the key [3′-^{2}H] KIE in the *sp*MTAN TS structure (Table 1). The dissociative S_N1 TS resembles that solved earlier without the 3′ KIE constraint.[15a] However, the [3′-^{2}H] KIE revealed the characteristic C1′→C4′ dihedral angles to form a nearly planar ribosyl pucker at the *sp*MTAN TS (Figures 2, 3). This ribosyl configuration is distinct from those of the reactant MTA and from the energetic minima of a fully developed ribooxacarbenium ion, whose H3′ conformation prefers an *endo* or *exo* geometry (Figure 3). Consequently, it is most appropriate to describe the *sp*MTAN TS with a geometry between the unrestrained H3′-*endo* MTA substrate and a fully developed 3′-*exo* ribooxacarbenium ion. This character distinguishes it from other reported MTAN transition states.[13,14,15a] The [3′-^{2}H] KIE defines the *sp*MTAN TS with modest 3′-OH polarization through a hydrogen bond between E174 of MTAN and the 3′-OH, similar to that seen in the crystal structure with a transition-state analogue inhibitor.[19] The degree of 3′-OH polarization was defined by the magnitude of the [3′-^{2}H] KIE. The hydrogen bond distance of 2.83 Å between MTA 3′-OH and the MTAN E174 supports polarization rather than complete 3′-OH ionization at the *sp*MTAN TS. The calculated hydrogen bond distance is within crystallographic error of the 2.6 to 2.7 Å extracted from crystal structures of MTANs bound to TS analogue inhibitors.[19,21] The 3′-OH polarization at *sp*MTAN TS is weaker than previously estimated.[15] The present results provide more reliable data since the previous interpretation relied on the indirect [4′-^{3}H] KIE that is sensitive to local geometries at the *sp*MTAN TS.

Accumulated evidence supports enzymatic dynamic motions in promoting catalysis, and computational chemistry can suggest TS structures.[22−24] However, experimental validation of the TS structure is best provided by KIE constraints. TS geometry comparisons from modeling and KIE approaches can then be

valuable. The well-characterized *sp*MTAN TS provides an opportunity to compare the structural difference between the TS and free reactant MTA. Structural changes of the *sp*MTAN TS relative to MTA involve C1′−N9 purine dissociation (region **III**, blue), ribosyl pucker reconfiguration (region **II**, red), and 5′-methylthio orientation (region **I**, black) (Figure 3). The geometry of the 5′-methylthio moiety at the *sp*MTAN TS is unlikely to be changed from the substrate−enzyme Michaelis complex. The fixed 5′-geometry prior to transition state formation has been observed for several N-ribosyl transferase enzymes.[13,15,25]

The structure of the *sp*MTAN TS is a fully dissociated adenylate anion and a ribosyl cation with the H3′-*endo*→*exo* conformation. *Complete* C1′−N9 dissociation with *incomplete* ribosyl reconfiguration to that expected for full carbocation development at the *sp*MTAN TS indicates coupled purine dissociation and carbocation formation before permitting full ribosyl cation geometric reorganization. Catalytic site contacts between *sp*MTAN and its transition-state mimic MT-ImmA reveal several key interactions in TS stabilization. The purine moiety in that structure forms hydrogen bonds with D197 and V152, while the ribosyl oxygens interact with E174, S76, R193, and M173.[19] The *sp*MTAN TS features, together with catalytic site contacts, suggest that contacts to the adenine leaving group promote purine dissociation rather than ribosyl ring conversion to the ribocation driving expulsion of the adenine.

Polarization of the 3′-OH at the *sp*MTAN TS is attributed to the hydrogen bond between the MTA 3′-OH moiety and E174,[19] which increases the 3′-OH bond length by 0.05 Å on the path to the TS. Polarizing the 3′-OH may play an essential role for MTAN TS formation since the oxacarbenium ion character can be stabilized by the more electronegative 3′ hydroxyl. Electron delocalization through the 2′-CH/4′-CH antibonding orbitals weakens 2′-CH/4′-CH bonds at the *sp*MTAN TS. The loss of 2′-CH/4′-CH bond order is consistent with the 2−4% KIEs contributed by 3′-OH polarization at these positions (discussion above and Table 1). 3′-Deoxy-MTA is a poor substrate for both *S. pneumoniae* and *E. coli* MTANs, giving slightly compromised K_m values but more than 10^3-fold decreased k_{cat}.[26,27] The preferential effect on k_{cat} rather than K_m indicates that the 3′-OH group of MTA is a key player for stabilizing transition states. Thus, partial 3′-OH polarization is exploited by MTAN isozymes for TS stabilization.

Synthesis of [3′-^{2}H]MTA permitted the measurement of the key [3′-^{2}H] KIE for *sp*MTAN-catalyzed hydrolysis. Addition of the [3′-^{2}H] KIE permits analysis of the ribosyl pucker geometry and the extent of the 3′-OH polarization or ionization at the TS of *sp*MTAN. The TS for *sp*MTAN reveals complete purine dissociation and incomplete ribosyl reconfiguration. Preferential interactions with the purine moiety are confirmed by loss of the purine prior to formation of a fully energy-equilibrated ribocation geometry via H3′-*endo*→*exo* ribosyl reconfiguration. No water nucleophilic participation is present at the TS; therefore this reaction, formally a nucleophilic displacement by water, occurs by a dissociative S_N1 mechanism followed by reorganization of the ribosyl causing C1′ to migrate toward the water and a late participation of water attack. This sequence of events characterizes the *sp*MTAN mechanism as "nucleophilic displacement by electrophile migration", a mechanism common to many glycosyl transferases.[24] This work provides new insights for understanding TS stabilization of MTAN-catalyzed reactions.

Acknowledgment. We thank Dr. Sean M. Cahill at the Albert Einstein College of Medicine for ^{1}H NMR experiments and Prof. Jiali Gao of the University of Minnesota Supercomputer Institute for computer time. This work was supported by NIH Grant GM41916.

Supporting Information Available: Detailed methods, Figure S1, and all optimized structures. This material is available free of charge via the Internet at http://pubs.acs.org.

References

(1) Wolfenden, R.; Snider, M. J. *Acc. Chem. Res.* **2001**, *34*, 938–945.
(2) Schramm, V. L. *J. Biol. Chem.* **2007**, *282*, 28297–28300.
(3) Wolfenden, R. *Biophys. Chem.* **2003**, *105*, 559–572.
(4) Schramm, V. L. *Arch. Biochem. Biophys.* **2005**, *433*, 13–26.
(5) Lewandowicz, A.; Schramm, V. L. *Biochemistry* **2004**, *43*, 1458–1468.
(6) Kim, K.; Cole, P. A. *J. Am. Chem. Soc.* **1997**, *119*, 11096–11097.
(7) Nikolic-Hughes, I.; Rees, D. C.; Herschlag, D. *J. Am. Chem. Soc.* **2004**, *126*, 11814–11819.
(8) Luo, M.; Li, L.; Schramm, V. L. *Biochemistry* **2008**, *47*, 2565–2576.
(9) Luo, M.; Schramn, V. L. *J. Am. Chem. Soc.* **2008**, *130*, 2649–2655.
(10) Schramm, V. L. *Curr. Opin. Chem. Biol.* **2007**, *11*, 529–536.
(11) Cleland, W. W. *Arch. Biochem. Biophys.* **2005**, *433*, 2–12.
(12) Luo, M.; Singh, V.; Taylor, E. A.; Schramm, V. L. *J. Am. Chem. Soc.* **2007**, *129*, 8008–8017.
(13) Singh, V.; Lee, J. E.; Nunez, S.; Howell, P. L.; Schramm, V. L. *Biochemistry* **2005**, *44*, 11647–11659.
(14) Singh, V.; Luo, M.; Brown, R. L.; Norris, G. E.; Schramm, V. L. *J. Am. Chem. Soc.* **2007**, *129*, 13831–13833.
(15) (a) Singh, V.; Schramm, V. L. *J. Am. Chem. Soc.* **2007**, *129*, 2783–2795. (b) Lee, J. E.; Settembre, E. C.; Cornell, K. A.; Riscoe, M. K.; Sufrin, J. R.; Ealick, S. E.; Howell, P. L. *Biochemistry* **2008**, *47*, 5159–5169.
(16) Gutierrez, J. A.; Luo, M.; Singh, V.; Li, L.; Brown, R. L.; Norris, G. E.; Evans, G. B.; Furneaux, R. H.; Tyler, P. C.; Painter, G. F.; Lenz, D. H.; Schramm, V. L. *ACS Chem. Biol.* **2007**, *2*, 725–734.
(17) Schauder, S.; Shokat, K.; Surette, M. G.; Bassler, B. L. *Mol. Microbiol.* **2001**, *41*, 463–476.
(18) Singh, V.; Evans, G. B.; Lenz, D. H.; Mason, J. M.; Clinch, K.; Mee, S.; Painter, G. F.; Tyler, P. C.; Furneaux, R. H.; Lee, J. E.; Howell, P. L.; Schramm, V. L. *J. Biol. Chem.* **2005**, *280*, 18265–18273.
(19) Singh, V.; Shi, W. X.; Almo, S. C.; Evans, G. B.; Furneaux, R. H.; Tyler, P. C.; Painter, G. F.; Lenz, D. H.; Mee, S.; Zheng, R. J.; Schramm, V. L. *Biochemistry* **2006**, *45*, 12929–12941.
(20) Singh, V.; Schramm, V. L. *J. Am. Chem. Soc.* **2006**, *128*, 14691–14696.
(21) Lee, J. E.; Singh, V.; Evans, G. B.; Tyler, P. C.; Furneaux, R. H.; Cornell, K. A.; Riscoe, M. K.; Schramm, V. L.; Howell, P. L. *J. Biol. Chem.* **2005**, *280*, 18274–18282.
(22) Fedorov, A.; Shi, W.; Kicska, G.; Fedorov, E.; Tyler, P. C.; Furneaux, R. H.; Hanson, J. C.; Gainsford, G. J.; Larese, J. Z.; Schramm, V. L.; Almo, S. C. *Biochemistry* **2001**, *40*, 853–860.
(23) Saen-Oon, S.; Ghanem, M.; Schramm, V. L.; Schwartz, S. D. *Biophys. J.* **2008**, *94*, 4078–4088.
(24) Schramm, V. L.; Shi, W. *Curr. Opin. Struct. Biol.* **2001**, *11*, 657–665.
(25) Murkin, A. S.; Birck, M. R.; Rinaldo-Matthis, A.; Shi, W.; Taylor, E. A.; Almo, S. C.; Schramm, V. L. *Biochemistry* **2007**, *46*, 5038–5049.
(26) (a) Allart, B.; Gatel, M.; Guillerm, D.; Guillerm, G. *Eur. J. Biochem.* **1998**, *256*, 155–162. (b) Kung, P. P.; Zehnder, L. R.; Meng, J. J.; Kupchinsky, S. W.; Skalitzky, D. J.; Johnson, M. C.; Maegley, K. A.; Ekker, A.; Kuhn, L. A.; Rose, P. W.; Bloom, L. A. *Bioorg. Med. Chem. Lett.* **2005**, *15*, 2829–2833.

JA804578M